Deferoxamine mitigates neuronal loss following spinal cord injury via ferroptosis inhibition and Nrf2/HO-1 pathway activation

ZIQIAN MA[1*], XINWEI ZHANG[1*], TAO LIU[1], YAN ZHANG[1], GUANGHAO LI[1], XIN YUAN[1], BENQIANG TANG[1], HANGYI ZHAO[2], LIANG LIU[1] and XUEMING CHEN[1]

[1]Department of Orthopedics Surgery, Beijing Luhe Hospital, Capital Medical University, Beijing 101149, P.R. China; [2]Department of Luhe Clinical Medical College, Capital Medical University, Beijing 101149, P.R. China

Received October 14, 2025; Accepted January 23, 2026

DOI: 10.3892/ijmm.2026.5808

Abstract. Spinal cord injury (SCI) is a debilitating condition associated with significant morbidity and permanent disability. The neuroprotective potential of deferoxamine (DFO) in SCI by targeting ferroptosis has been highlighted; however, the underlying molecular mechanisms remain elusive. The present study aimed to investigate the role of the Nrf2/heme oxygenase-1 (HO-1) signaling pathway in mediating the inhibitory effects of DFO on neuronal ferroptosis following SCI. The study commenced with a bioinformatics analysis of the SCI microarray dataset, GSE162610. Kyoto Encyclopedia of Genes and Genomes pathway analysis indicated significant activation of ferroptosis following SCI, while Gene Ontology analysis revealed that oxidative stress, inflammatory response and glutathione peroxidase activity were key biological processes associated with ferroptosis post-SCI. The Nrf2, glutathione peroxidase 4 (GPX4), HO-1 (encoded by Hmox1) and xCT (encoded by Slc7a11) genes were selected for further investigation. Subsequent experiments employed the Nrf2-specific inhibitor ML385 to evaluate the regulatory role of the Nrf2/HO-1 pathway. *In vitro*, an erastin-induced neuronal ferroptosis model was established using ventral spinal cord 4.1 cells, while *in vivo*, a spinal cord contusion model was constructed using C57BL/6J mice for behavioral, histopathological and immunological assessments. The results demonstrated that, compared with the SCI group, DFO treatment significantly upregulated the expression of Nrf2, HO-1, xCT and GPX4 both *in vitro* and *in vivo* as well as attenuated neuronal loss and tissue damage and promoted motor functional recovery in mice. Conversely, the administration of ML385 largely reversed these molecular and functional effects of DFO, thereby diminishing its neuroprotective efficacy. These findings indicated that DFO alleviated neuronal ferroptosis and promoted functional recovery after SCI, at least in part, through activation of the Nrf2/HO-1 signaling pathway and enhancement of the xCT/GPX4 antioxidant system. Therefore, the present study elucidated the involvement of the Nrf2/HO-1 signaling pathway in mediating the neuroprotective effects of DFO in SCI, highlighting the therapeutic potential of DFO and providing a theoretical foundation for future targeted strategies against ferroptosis in SCI management.

Correspondence to: Professor Liang Liu or Professor Xueming Chen, Department of Orthopedics Surgery, Beijing Luhe Hospital, Capital Medical University, 82 Xinhua South Road, Tongzhou, Beijing 101149, P.R. China
E-mail: liuliang@ccmu.edu.cn
E-mail: chenxueming@ccmu.edu.cn

*Contributed equally

Key words: spinal cord injury, ventral spinal cord 4.1 cells, ferroptosis, deferoxamine, Nrf2/heme oxygenase-1 signaling pathway, bioinformatics

Introduction

Spinal cord injury (SCI) is a traumatic condition that imposes notable physical, emotional and economic burdens on patients and their families. An epidemiological meta-analysis showed that the incidence of traumatic SCI in developing countries was 22.55 per million individuals per year (1). The pathogenesis of SCI is well understood and involves primary and secondary injuries. Primary injury occurs immediately following trauma and typically involves mechanical damage, either permanent or temporary compression (2,3). Secondary injury, characterized by destructive biochemical changes within the spinal cord, including neuroinflammation, cell death, blood vessel injury, disruption of the blood-spinal cord barrier and oxidative stress, further exacerbates tissue damage and functional impairment (4,5). Despite extensive research into various treatment modalities such as pharmacotherapy, stem cell therapy, biomaterials and rehabilitation, effective treatments for SCI remain elusive (6-8).

Cell death, particularly neuronal death, is a critical factor contributing to functional deficits following SCI. Therefore, strategies aimed at preventing neuronal death may hold promise for ameliorating post-SCI pathology. Various types of cell death have been reported in SCI, including necroptosis, apoptosis, autophagy, ferroptosis, pyroptosis and paraptosis (9). Ferroptosis is a recently discovered form of regulated cell death defined by iron-dependent lipid peroxidation (10). Glutathione peroxidase 4 (GPX4), cystine/glutamate antiporter

(System Xc-) and glutathione (GSH) collectively constitute the System Xc-/GSH/GPX4 axis, which is crucial in mitigating excessive lipid peroxidation and reducing reactive oxygen species generation in ferroptosis (11). Our previous studies have revealed the engagement of ferroptosis in SCI pathogenesis and highlighted the therapeutic potential of ferroptosis inhibitors in promoting functional recovery in SCI animal models (12,13). Moreover, previous studies have underscored the significance of the System Xc-/GSH/GPX4 axis in regulating ferroptosis after SCI, consistent with findings from other research groups (14-16).

Deferoxamine (DFO), an Food and Drug Administration (FDA)-approved iron-chelating agent, has been shown in our previous study to prevent ferroptosis and promote functional recovery in SCI mice (12). Additionally, DFO has been demonstrated to reverse erastin-induced neuronal ferroptosis in primary cortical neurons (17). Although the efficacy of DFO in treating SCI by inhibiting ferroptosis has been established, the underlying molecular mechanisms remain incompletely understood.

Previous studies have suggested that various compounds, including zinc, trehalose and resveratrol, promote functional recovery after SCI by inhibiting ferroptosis through upregulation of the Nrf2 gene. Specifically, Ge *et al* (18) explored the role of zinc in SCI and found that it attenuates ferroptosis and promotes functional recovery by activating the Nrf2/GPX4 defense pathway. This study underscored the importance of the Nrf2 pathway in mitigating ferroptosis and aiding recovery after SCI. Gong *et al* (19) also reported that trehalose inhibits ferroptosis in an SCI mouse model by activating the Nrf2/heme oxygenase-1 (HO-1) pathway. Their findings suggested that the Nrf2/HO-1 axis plays a crucial role in protecting neurons from ferroptosis and enhancing functional recovery. Ni *et al* (20) found that resveratrol inhibits ferroptosis via activation of the Nrf2/GPX4 pathway in mice with SCI. This study further supported the involvement of the Nrf2 pathway in reducing ferroptosis and promoting recovery post-SCI. These studies collectively highlight the Nrf2 signaling pathway as a key regulator in inhibiting ferroptosis and promoting functional recovery in SCI. By activating components of the Nrf2 pathway, such as GPX4 and HO-1, various compounds, including zinc, trehalose and resveratrol, offer neuroprotection and facilitate recovery following SCI. This suggests that targeting the Nrf2 pathway could be a promising therapeutic strategy for mitigating ferroptosis and enhancing outcomes in SCI. Despite the well-documented role of the Nrf2/HO-1 signaling pathway in modulating oxidative stress and ferroptosis, the specific interaction between DFO and this pathway in the context of SCI remains largely unexplored. Previous studies have primarily focused on the general effects of Nrf2 activation in oxidative stress and ferroptosis, but the direct involvement of the Nrf2/HO-1 axis in mediating the neuroprotective effects of DFO after SCI has not been fully elucidated (21,22). This gap in knowledge presents an opportunity to explore the intricate molecular crosstalk between DFO and the Nrf2/HO-1 pathway, thereby advancing our understanding of the mechanistic basis of the therapeutic potential of DFO in SCI.

The present study aimed to elucidate the role of the Nrf2/HO-1 signaling pathway in mediating the inhibitory effects of DFO on neuronal ferroptosis after SCI. To achieve this goal, an SCI mouse model was employed to investigate alterations in Nrf2 expression following DFO administration. Additionally, the Nrf2-specific inhibitor, ML385, was utilized to elucidate the engagement of the Nrf2/HO-1 signaling pathway in the molecular mechanisms underlying DFO treatment.

Materials and methods

Animals. Female C57BL/6 J Nifdc mice weighing 20-25 g and aged 6-8 weeks were procured from Beijing Vital River Laboratory Animal Technology Co., Ltd. [License SCXK (Jing) 2021-0011]. To eliminate potential sex-related variations and reduce the risk of urinary tract infections, only female mice were included in the present study. The mice were kept in standard cages with a 12-h light-dark cycle, with 5 mice per cage. Adequate water and food were supplied *ad libitum* and the ambient temperature was maintained between 22 and 24˚C. Prior to the commencement of the experimental procedures, the mice were housed to acclimatize to their surroundings for 1 week. Ethical approval for the study was obtained from the Animal Experiments and Experimental Animal Welfare Committee of Capital Medical University (Beijing, China; approval no. AEEI-2023-029, granted on March 8, 2023). All procedures were performed according to the guidelines stipulated by the Animal Research: Reporting of *in vivo* Experiments (ARRIVE) (23).

SCI model and treatment. The SCI model was established following the protocol outlined in a previous study (24). In brief, mice were anesthetized with a combination of isoflurane (Lunan Pharmaceutical Group Limited) and air (4% isoflurane for induction and 2% for maintenance). A total of 60 mice were randomly assigned to one of four groups: The Sham, SCI, SCI + DFO injection (DFO group) and SCI + DFO with ML385 injection (ML385 group) groups (n=15 per group). To establish the SCI model, mice were anesthetized and maintained with isoflurane. Subsequently, each mouse was positioned on the operating table in a prone position. A laminectomy was performed to expose the T9/T10 vertebral region and the dorsal tissue of the spinal cord was fully exposed. SCI was induced using a weight-dropping method with an IMPACTOR MODEL III (procured from State University of New Jersey, New Brunswick, NJ, USA), utilizing a 30 mm high, 5 g weight and 2 mm diameter rod. The incision was then closed with sterile sutures. Mice in the Sham group only underwent laminectomy without spinal cord damage. Successful induction of SCI was confirmed by bilateral hind limb paralysis in the mice. Throughout the experiment, the animals were monitored every day for general health, cage activity and signs of infection. Bladder urination was completed twice daily during the first week post-surgery. Mice in the DFO and ML385 groups received intraperitoneal injections of DFO (100 mg/kg; once daily for 3 consecutive days) and mice in the ML385 group additionally received ML385 (30 mg/kg; once daily for 3 consecutive days). The doses of DFO and ML385 were selected based on previous studies in which these regimens effectively reduced ferroptosis and modulated Nrf2 signaling *in vivo* without causing notable toxicity in mice (12,25). Mice in the SCI and Sham groups received equivalent intraperitoneal

injections of 0.9% NaCl, also administered once daily until the third day post-modeling. Animals were monitored at least once daily throughout the study and more frequently during the first 72 h post-injury. Predefined humane endpoints for early euthanasia included: i) >20% loss of preoperative body weight or progressive weight loss with dehydration despite supportive care; ii) inability to reach food/water or failure to thrive; iii) severe or unrelieved pain/distress not responsive to analgesia/supportive care; iv) severe wound complications (such as dehiscence, uncontrolled bleeding, infection, pressure sores or autophagia); and v) moribund condition (such as minimal responsiveness or other signs of impending death as assessed by trained personnel). If any criterion had been met, animals would have been euthanized immediately in accordance with institutional guidelines. However, no animals reached the predefined humane endpoints before completion of the planned study period.

Behavioral testing. For behavioral assessment, 6 mice per group were followed longitudinally, and Basso Mouse Scale (BMS) scores and subscores were recorded at 1, 3, 5, 7, 14, 21 and 28 days post-injury. The BMS hindlimb locomotor rating system, as described by Basso *et al* (26), was employed to assess the functional recovery of the mice. The BMS scores range from 0 to 9 points, with 0 indicating complete paralysis and 9 representing normal function. Assessment criteria encompassed observations of range of motion, frequency of hindlimb plantar stepping, rear ankle joint activities, coordination, touch response of the soles of the feet and insteps, foot position, trunk stability and tail position. Additionally, BMS subscores ranging from 0 to 11 were assessed concurrently. To minimize the potential influence of bladder fullness, manual bladder expression was performed 2 h prior to BMS evaluations. The evaluators were blinded to the experimental conditions of the mice and assessments were conducted three times with immediate recording. All personnel involved underwent rigorous training to ensure consistency and accuracy in the assessments.

Tissue preparation. At 2 (n=6 per group) and 28 (n=9 per group) days post-surgery, the spinal cord tissue was harvested from the mice of each experimental group. Animals were euthanized by isoflurane overdose (5% isoflurane in room air until cessation of breathing) and death was confirmed by the absence of heartbeat and the loss of corneal and pedal withdrawal reflexes prior to perfusion. Day 2 post-SCI was selected as an early acute-phase time point to assess rapid activation of oxidative stress responsive pathways (including Nrf2/HO-1) and the early effect of DFO, whereas day 28 was used to evaluate longer-term outcomes. This was followed by cardiac perfusion with 0.9% NaCl and 4% paraformaldehyde (PFA). Subsequently, spinal cord samples measuring 0.5 cm in length, containing the epicenter of the injury site, were carefully harvested. Samples designated for western blot analysis were washed with phosphate-buffered saline (PBS) and lysed using RIPA lysis buffer (Beijing Aoqing Biotechnology Co., Ltd.). Samples intended for immunofluorescence staining or histology staining were fixed in 4% PFA solution. Following fixation, a gradient dehydration process was carried out using sucrose solutions. The spinal cord tissues were embedded in Optimal Cutting Temperature Compound (Beijing Aoqing Biotechnology Co., Ltd.), frozen and cut into 10-μm longitudinal cryosections in a cryostat (CM1950; Leica Microsystems GmbH) with the chamber temperature set to -20˚C. These frozen sections were stored at -20˚C until further analysis.

Western blotting. Western blotting was performed according to our previous study (27). For each time point, spinal cord samples from 3 mice per group were pooled and analyzed. For each sample, 20-30 μg of protein was mixed with 5X SDS-PAGE loading buffer (Beyotime Biotechnology) and boiled at 95˚C for 5 min. The samples were then loaded onto a 10% SDS-PAGE gel and separated by electrophoresis at 80 V for stacking and 120 V for resolving. After electrophoresis, the proteins were transferred to PVDF membranes (MilliporeSigma) at 300 mA for 90 min using a wet transfer system (Bio-Rad Laboratories, Inc.). Following the transfer, membranes were blocked with 5% non-fat milk in Tris-buffered saline with 0.1% Tween-20 (TBST) for 1 h at room temperature. The membranes were then incubated with primary antibodies overnight at 4˚C. The primary antibodies used were: Anti-Nrf2 (1:1,000; CST Biological Reagents Co., Ltd.; cat. no. 12721S), anti-HO-1 (1:1,000; Abcam; cat. no. ab68477), anti-GPX4 (1:1,000; Abcam; cat. no. ab41787), anti-xCT (1:5,000; Abcam; cat. no. ab175186) and β-actin (1:1,000; Abcam; cat. no. ab8227). After primary antibody incubation, the membranes were washed three times with TBST for 10 min each and then incubated with horseradish peroxidase-conjugated secondary antibodies [1:5,000; Beijing Huaxing Bocheng Gene Technology Co., Ltd.; cat. nos. HX2031 (rabbit) and HX2032 (mouse)] for 1 h at room temperature. The membranes were washed again with TBST three times for 10 min each. Immunoreactive bands were visualized using BeyoECL Plus (Beyotime Biotechnology) according to the manufacturer's instructions. The chemiluminescent signals were detected and captured using the ChemiDoc XRS+ imaging system (Bio-Rad Laboratories, Inc.). Densitometric analysis of the bands was performed using ImageJ2X software (National Institutes of Health). The expression levels of target proteins were normalized to β-actin as the loading control.

VSC4.1 cell culture. The effects of DFO on the expression of the Nrf2/HO-1 signaling pathway were validated with an *in vitro* erastin-induced neuronal ferroptosis model using the rat VSC4.1 cell line, created as previously described (18). VSC4.1 is an immortalized motor neuron-like hybrid cell line that has been described as a motoneuron-neuroblastoma fusion product (28). The cells were purchased from Hunan Fenghui Biotechnology Co., Ltd. (cat. no. CL0674) and cultured at 37˚C with 5% CO_2 in Dulbecco's Modified Eagle Medium (Procell Life Science & Technology Co., Ltd.; cat. no. PM150220) supplemented with 10% fetal bovine serum (Gibco; Thermo Fisher Scientific, Inc.) and 1% penicillin-streptomycin. The VSC4.1 cells were divided into four groups: The Control, Erastin, DFO and ML385 groups. In the Erastin group, VSC4.1 cells were treated with erastin (10 μM) for 24 h. In the DFO group, VSC4.1 cells were treated with a combination of erastin (10 μM) and DFO (10 μM) for 24 h. For the ML385 group, an inhibitor of the Nrf2 signaling pathway, ML385 (5 μM), was also added to DFO treatment for 24 h (29). The Control

group was cultured in culture medium without any additional treatment. The Control group served as a baseline to evaluate the effects of erastin-induced ferroptosis and the subsequent protective effects of DFO and the impact of Nrf2 inhibition by ML385. All other culture conditions and parameters remained consistent across all experimental groups.

Immunofluorescence staining. Immunofluorescence staining of spinal cord tissue was performed on sections obtained from 6 mice per group at the indicated time points. Frozen spinal cord sections were allowed to equilibrate to room temperature for 1 h. Sections were then washed three times with PBS for 5 min each to remove any residual embedding medium. The sections were permeabilized and blocked by incubating them in a solution containing 0.5% Triton X-100 and 1% bovine serum albumin (BSA) (Thermo Fisher Scientific, Inc.) in PBS for 2 h at room temperature. This step reduces non-specific antibody binding and permeabilizes the tissue to allow antibody penetration. After blocking, the sections were incubated with the following primary antibodies diluted in PBS containing 1% BSA: Anti-Nrf2 (1:250; CST Biological Reagents Co., Ltd.; cat. no. 12721S), anti-GPX4 (1:300; Abcam; cat. no. ab41787) and anti-Tuj1 (1:250; Abcam; cat. no. ab78078). The sections were incubated with the primary antibodies overnight at 4˚C to ensure optimal binding. The next day, sections were washed three times in PBS (5 min each) and then incubated with fluorophore-conjugated secondary antibodies diluted in PBS containing 1% BSA for 2 h at room temperature in the dark, including Alexa Fluor 488-conjugated goat anti-rabbit IgG (H+L) (1:500; Abcam; cat. no. ab150077) and Rhodamine (TRITC)–conjugated goat anti-mouse IgG (H+L) (1:500; Proteintech Group, Inc.; cat. no. SA00007-1). Following secondary antibody incubation, the sections were washed three times with PBS for 5 min each. The sections were then stained with 4',6-diamidino-2-phenylindole (DAPI) for 10 min at room temperature to label cell nuclei. After the final wash with PBS, the sections were mounted with an antifade mounting medium to preserve fluorescence and minimize photobleaching. The stained sections were visualized and imaged using a laser scanning confocal microscope (Nikon Corporation). Z-stack images were captured for three-dimensional analysis where necessary. Representative images were analyzed using ImageJ software (National Institutes of Health), and fluorescence intensity was quantified to assess protein expression levels.

For cellular experiments, the ventral spinal cord 4.1 (VSC4.1) cells were seeded into 24-well plates pre-coated with poly-D-lysine (Sigma-Aldrich; Merck KGaA). After the experimental treatments, the cells were washed three times with 1X PBS, 5 min per wash, to remove any residual medium and treatment agents. Cells were fixed with 4% PFA for 15 min at room temperature to preserve cellular structure. Following fixation, cells were permeabilized and blocked with a solution containing 0.1% Triton X-100 and 0.5% BSA in PBS for 30 min at room temperature to reduce non-specific binding. The fixed and permeabilized cells were incubated with the aforementioned primary antibodies diluted in PBS containing 1% BSA. The cells were incubated overnight at 4˚C to allow adequate antibody binding. After three washes with PBS, the cells were incubated with the aforementioned fluorophore-conjugated secondary antibodies diluted in PBS with 1% BSA for 1 h at room temperature in the dark. Cells were stained with DAPI for 10 min at room temperature to label nuclei. After the final washes, the cells were kept in PBS for imaging. Images were captured using a confocal microscope and representative fields were analyzed with ImageJ software for fluorescence intensity quantification.

Hematoxylin and eosin (H&E) and Nissl staining. At 28 days post-injury, spinal cord tissues (n=6 per group) were harvested and subjected to standard histopathological processing for H&E and Nissl staining according to established protocols.

For H&E staining, first, the cryopreserved spinal cord sections were equilibrated to room temperature for thawing. Nuclear staining was then performed by incubation in hematoxylin solution (Beijing Solarbio Science & Technology Co., Ltd.) (3 min at room temperature), resulting in characteristic blue-purple nuclear chromatin visualization. Following differentiation, cytoplasmic counterstaining was achieved using eosin solution for 1 min at room temperature to demonstrate pink-red cytoplasmic components. Subsequent dehydration was performed through a graded ethanol series, with xylene clearing for tissue transparency. Sections were permanently mounted using neutral resin mounting medium prior to bright-field microscopic examination. Histological damage scoring based on edema, neutrophil infiltration and hemorrhage was as follows: 0 points, asymptomatic or mild; 1 point, limited; 2 points, moderate; 3 points, prominent; and 4 points, extensive. For each section, the three components were scored separately and then averaged (range 0-4) to obtain an overall damage score. Scores were independently calculated by two pathologists and averaged to obtain the final values.

For Nissl staining, after similar thawing procedures, sections were processed using standardized Nissl staining reagents (Wuhan Servicebio Technology Co., Ltd.). The staining protocol included differentiation in glacial acetic acid solution to optimize Nissl staining contrast. Nissl staining was performed by incubating sections in cresyl violet for 5 min at room temperature. Following air-drying, sections were similarly mounted with neutral resin for microscopic evaluation of neuronal architecture and Nissl staining distribution.

Source of the gene datasets, data collection and analyses. The present study performed bioinformatics analyses using the publicly available dataset GSE162610 (https://www.ncbi.nlm.nih.gov/geo/) deposited in the NCBI Gene Expression Omnibus (GEO) database, which contains single-cell RNA sequencing data from uninjured and injured mouse spinal cords at 1, 3, and 7 days post-injury, originally generated by Milich *et al* (30). The raw expression matrix was processed and analyzed in the R programming environment (version 4.3.1; R Core Team; https://www.r-project.org/) for subsequent statistical analysis. The following programs and their respective versions were used for each analysis: readxl (version 1.4.5, for reading Excel files), ggplot2 (version 4.0.1, for data visualization), cluster Profiler (version 4.2.2, Bioconductor Release 3.13, for differential expression analysis and functional enrichment), enrich plot (version 1.30.4, Bioconductor, for visualizing enrichment analysis results) and org.Mm.eg.db (version 3.22.0, Bioconductor, for mouse genome annotation). Differentially expressed genes (DEGs) were identified by comparing the gene

expression levels between the injury and control groups using a pairwise quasi-likelihood F-test. A significance threshold of P<0.05 was applied for statistical analysis and the pseudo-bulk method was used for differential analysis. Based on the selected DEGs, Gene Ontology (GO) and Kyoto Encyclopedia of Genes and Genomes (KEGG) pathway enrichment analyses were conducted and volcano plots were generated, highlighting genes specifically associated with ferroptosis. Furthermore, a protein-protein interaction (PPI) network was constructed using the STRING database (https://string-db.org/) (limited to *Mus musculus*) to obtain interaction data, which was then imported into Cytoscape for network visualization and topological analysis. Key node proteins were selected for further analysis. All figures were generated using GraphPad Prism 9.4.0 (Dotmatics).

Statistical analysis. Data were analyzed using GraphPad Prism (version 9.3; Dotamatics). All data are presented as the mean ± standard deviation. For single time-point outcomes involving more than two groups, one-way ANOVA was applied when assumptions of normality and homogeneity of variance were met, followed by Bonferroni post hoc testing for multiple comparisons. For two-group comparisons at a single time point in which the data were not normally distributed, the Mann-Whitney U test was used. For locomotor recovery, BMS scores were analyzed using a two-way repeated-measures ANOVA across the full time course, with treatment group as the between-subject factor and time (post-injury day) as the within-subject repeated factor, including assessment of the group x time interaction. When significant effects were detected, Tukey's post hoc test was performed to compare treatment groups at the same post-injury day. P<0.05 was considered to indicate a statistically significant difference.

Results

DFO protects neurons and activates the Nrf2/HO-1 signaling pathway after SCI. To assess changes in Nrf2/HO-1 expression following SCI and treatment with DFO in mice, western blotting was employed. As depicted in Fig. 1A-C, the expression of Nrf2 and HO-1 in the DFO-treated group significantly increased compared with the SCI group. Notably, the Nrf2/HO-1 expression levels showed a trend toward upregulation in the SCI group compared with the Sham group (P>0.05), suggesting a possible endogenous compensatory response to injury-associated oxidative stress. However, this trend was not statistically significant. Moreover, immunofluorescence staining demonstrated a significant increase in neuronal Nrf2 expression ($Tuj1^+$ cells) in the DFO-treated group compared with the SCI group at 2 days post-SCI (P<0.05; Fig. 1D and E).

DFO confers neuroprotection and enhances the expression of the Nrf2/HO-1 signaling pathway in an erastin-induced neuronal ferroptosis model. Neurons play a pivotal role in the pathogenesis of SCI and represent a potential target for treatment strategies. Western blotting analysis of VSC4.1 cells revealed that the expression levels of Nrf2 and HO-1 were significantly elevated in the DFO treatment group compared with the Erastin group (Fig. 2A-C). Similarly, erastin treatment tended to increase Nrf2 and HO-1 expression compared with the Control group; however, the differences did not reach statistical significance (P>0.05) (Fig. 2A-C). Immunofluorescence staining further demonstrated the neuroprotective effect of DFO on VSC4.1 cells. Specifically, Tuj1 (βIII-tubulin), a marker of neuronal phenotype and cytoskeletal/neurite integrity, was markedly reduced after Erastin exposure, whereas DFO treatment preserved Tuj1 signal (and/or the proportion of $Tuj1^+$ cells), indicating improved maintenance of neuronal structural identity (Fig. 2D-F).

DFO attenuates neuronal ferroptosis by modulating the xCT/GPX4 antioxidant system via activating the Nrf2/HO-1 signaling pathway in SCI mice. Previous investigations from our laboratory have demonstrated the efficacy of DFO in preventing neuronal ferroptosis by governing the xCT/GPX4 antioxidant system (12). However, the participation of the Nrf2/HO-1 signaling pathway in this process remains elusive. To address this question, ML385, an Nrf2 inhibitor, was employed to elucidate the role of Nrf2 in the DFO-mediated treatment of SCI in mice. The experimental design is outlined in Fig. 3A.

The BMS was utilized to assess open-field locomotion in SCI mice with assessments conducted at various time points post-injury. At 1 day post-injury, which was the first behavioral assessment time point, the BMS score was 0, supporting reliable establishment of the SCI model. Subsequent assessment revealed that the scores and sub-scores of mice in the DFO group were significantly higher than those in the SCI group and ML385 group at days 14, 21 and 28 post-injury (P<0.05). However, no significant differences were observed between the SCI group and ML385 group (Fig. 3B and C), suggesting that ML385 administration reversed the beneficial effects of DFO on functional recovery in SCI mice.

H&E staining showed that the SCI group had significant spinal cord damage, hemorrhage and edema compared with the DFO group at 28 days post-injury (P<0.05). ML385 administration appeared to attenuate spinal cord recovery compared with the DFO group, but this effect did not reach statistical significance (Fig. 3D and E). Nissl staining revealed that the SCI group exhibited significant tissue loss and neuronal damage. By contrast, the DFO group exhibited improved tissue integrity and reduced neuronal damage. However, these beneficial effects were diminished in the ML385-treated group (P<0.05; Fig. 3F and G). These findings suggest that DFO-Nrf2 signaling pathway may mitigate tissue loss and neuronal injury following SCI.

Further examination via western blotting revealed that the expression levels of Nrf2 and HO-1 were significantly downregulated in the ML385 group compared with the DFO group (Fig. 4A-C). Conversely, DFO treatment led to a significant upregulation in the expression of xCT and GPX4 compared with the SCI group. However, the protein levels of xCT and GPX4 in the ML385 group were reduced compared with the DFO group (Fig. 4D-F), indicating a reversal of the effects of DFO by ML385.

Immunofluorescence analysis further supported these findings, evidenced by a significant decrease in the number of $Nrf2^+Tuj1^+$ neurons in the ML385 group compared with the DFO group (Fig. 4G and I). Additionally, DFO treatment significantly upregulated the expression of GPX4 in $Tuj1^+$

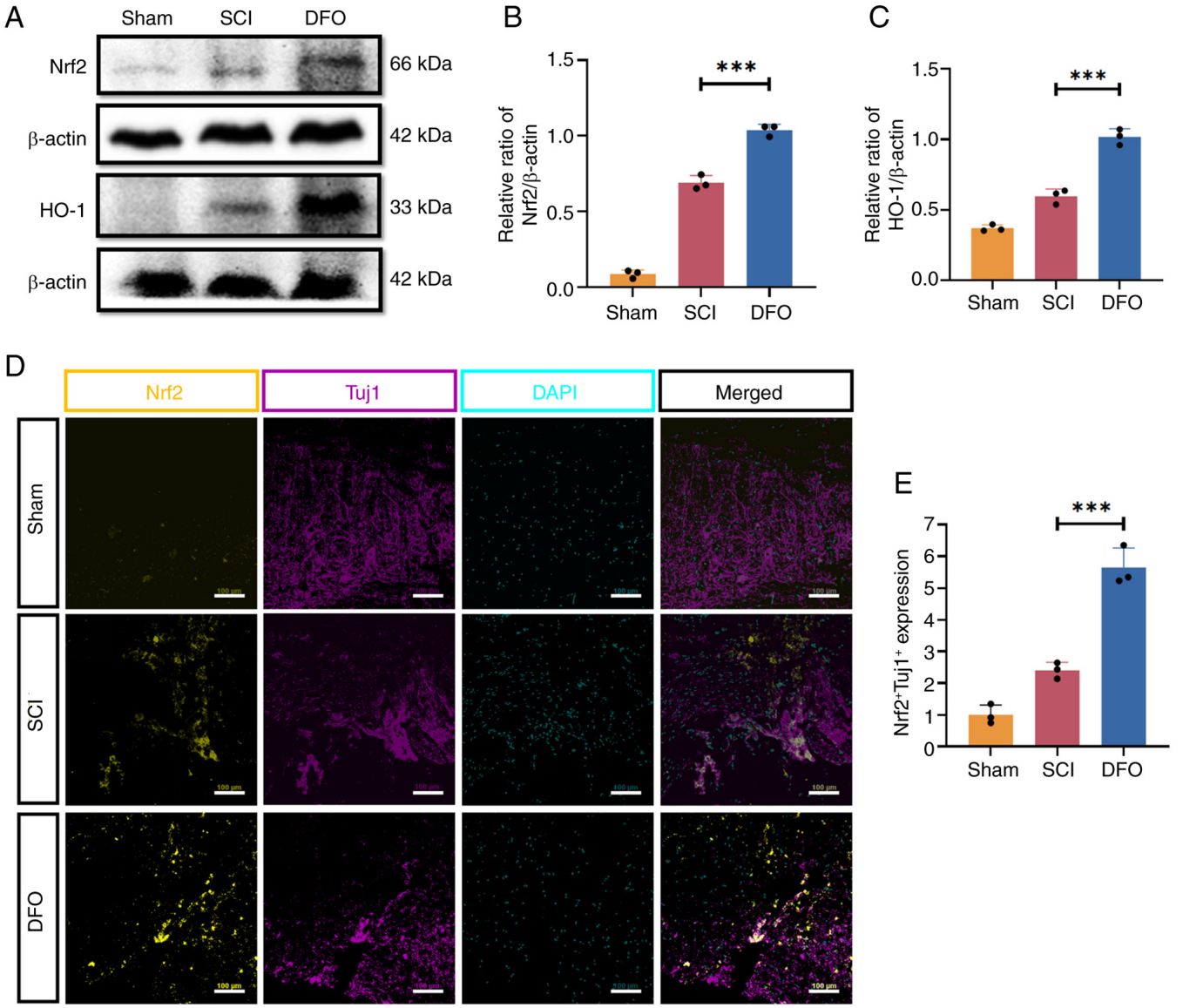

Figure 1. Effects of DFO on the Nrf2/HO-1 signaling pathway after SCI in mice. (A) Protein expression levels of Nrf2 and HO-1 at 2 days post-SCI were assessed by western blotting. Semi-quantification of the (B) Nrf2 and (C) HO-1 expression levels. (D) Immunofluorescence staining showing Nrf2 in Tuj1$^+$ neurons at 2 days post-SCI (scale bar, 100 μm). (E) Quantitative analysis of Nrf2$^+$ Tuj1$^+$ neurons in each group. Data are presented as the mean ± SD (n=3 per group). Statistical analysis was performed using one-way ANOVA followed by the Bonferroni post hoc test; ***P<0.001. DFO, deferoxamine; HO-1, heme oxygenase-1; SCI, spinal cord injury; DAPI, 4',6-diamidino-2-phenylindole.

neurons in spinal cord tissue, while ML385 administration attenuated this effect (Fig. 4H and J), further highlighting the role of Nrf2 in regulating the neuroprotective effects of DFO.

DFO inhibits erastin-induced neuronal ferroptosis by regulating the xCT/GPX4 antioxidant system via activation of the Nrf2/HO-1 signaling pathway. To elucidate the involvement of the Nrf2/HO-1 signaling pathway in DFO intervention *in vitro*, ML385 was introduced into VSC4.1 cells. Western blotting analysis revealed that the expression levels of Nrf2 and HO-1 were downregulated in the ML385 group compared with the DFO group (Fig. 5A-C). Additionally, the levels of the ferroptosis markers xCT and GPX4 were significantly higher in the DFO group compared with the Erastin group. However, following ML385 treatment, the expression of xCT and GPX4 was notably downregulated compared with the DFO group (Fig. 5D-F). Immunofluorescence analysis further corroborated these findings, demonstrating a significant upregulation of Nrf2 expression in VSC4.1 cells after DFO treatment compared with the Erastin group, while ML385 administration attenuated the levels of Nrf2 compared with the DFO group (Fig. 5G and H).

Analysis of a single-cell RNA sequencing dataset reveals dynamic activation of ferroptosis-related pathways after SCI. An unbiased overview of transcriptional alterations associated with SCI was obtained by analyzing the public dataset GSE162610, in which spinal cord tissues collected at 1, 3 and 7 days post-injury were compared with those from uninjured controls. KEGG pathway enrichment analysis demonstrated a clear time-dependent shift in biological programs following SCI. At 1 day post-injury, DEGs were

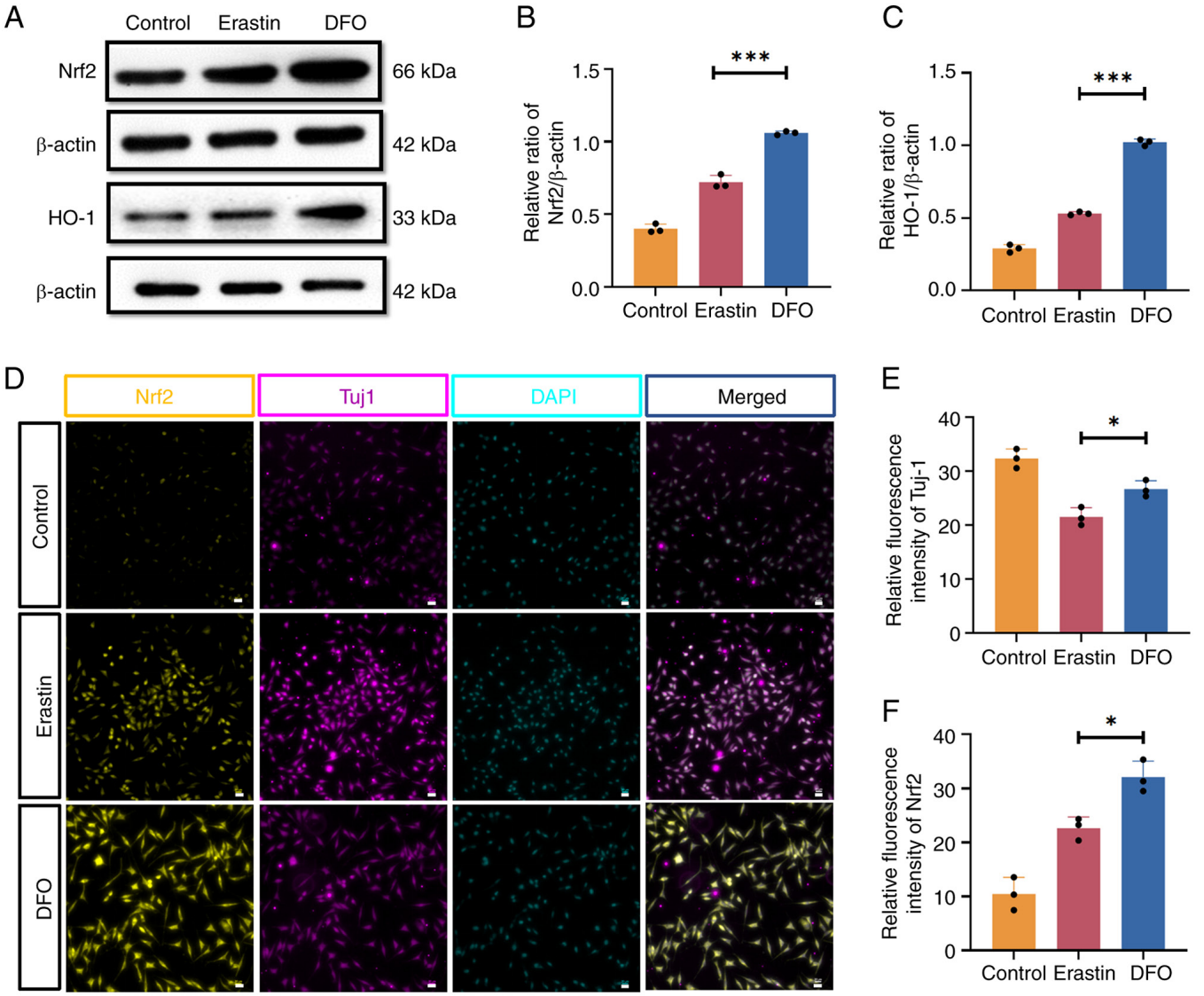

Figure 2. Effects of DFO on the expression of Nrf2 and HO-1 in the VSC 4.1 cell line after treatment with erastin. (A) Protein expression levels of Nrf2 and HO-1 in VSC4.1 cells from the Control, Erastin and DFO groups were evaluated by western blotting. Semi-quantification of the (B) Nrf2 and (C) HO-1 expression levels. (D) Immunofluorescence staining showing Nrf2 and Tuj1 in different groups (scale bar, 20 μm). Quantitative analysis of (E) Tuj1$^+$ and (F) Nrf2$^+$ VSC4.1 cells in different groups. Data are presented as the mean ± SD (n=3 per group). Statistical analysis was performed using one-way ANOVA followed by Bonferroni post hoc test; *P<0.05, ***P<0.001. DFO, deferoxamine; HO-1, heme oxygenase-1; VSC4.1, ventral spinal cord 4.1; DAPI, 4',6-diamidino-2-phenylindole.

mainly enriched in the MAPK, PI3K-AKT, TNF and NF-κB signaling pathways, together with pathways associated with apoptosis and HIF-1 signaling, reflecting an acute stress and inflammatory response (Fig. S1D). At 3 and 7 days post-SCI, enrichment progressively shifted toward immune-related pathways, including 'Cytokine-cytokine receptor interaction', 'Chemokine signaling pathway' and 'Leukocyte transendothelial migration'. Notably, the KEGG pathway 'Ferroptosis' was significantly enriched at 3 days (subacute phase) and 7 days (early chronic phase) post-SCI, suggesting persistent involvement of iron-dependent lipid peroxidation in SCI pathophysiology (Fig. 6A and B).

To further functionally characterize ferroptosis-associated transcriptional alterations after SCI, GO enrichment analysis was performed for DEGs at 1, 3 and 7 days post-injury. The predominant acute stress response at 1 day post-SCI was evidenced by the significant enrichment of GO biological process terms including 'response to oxidative stress' and 'regulation of inflammatory response' (Fig. S1B), together with molecular function terms such as 'ferrous iron binding' and 'peroxidase activity' (Fig. S1A and C). At 3 and 7 days post-SCI, GO enrichment revealed a more notable and consistent involvement of ferroptosis-related biological processes (Fig. 6G-L). In the biological processes category, enriched terms included 'response to oxidative stress', 'lipid oxidation', 'glutathione metabolic process' and 'cellular iron ion homeostasis'. In the cellular components category, DEGs were predominantly localized to 'mitochondrial matrix' and 'lysosomal membrane', suggesting sustained mitochondrial dysfunction and lipid turnover. Correspondingly, molecular functions analysis highlighted enrichment of 'glutathione peroxidase activity', 'antioxidant activity' and 'oxidoreductase activity, acting on metal ions'. Collectively, these GO enrichment patterns indicate persistent disruption of redox balance,

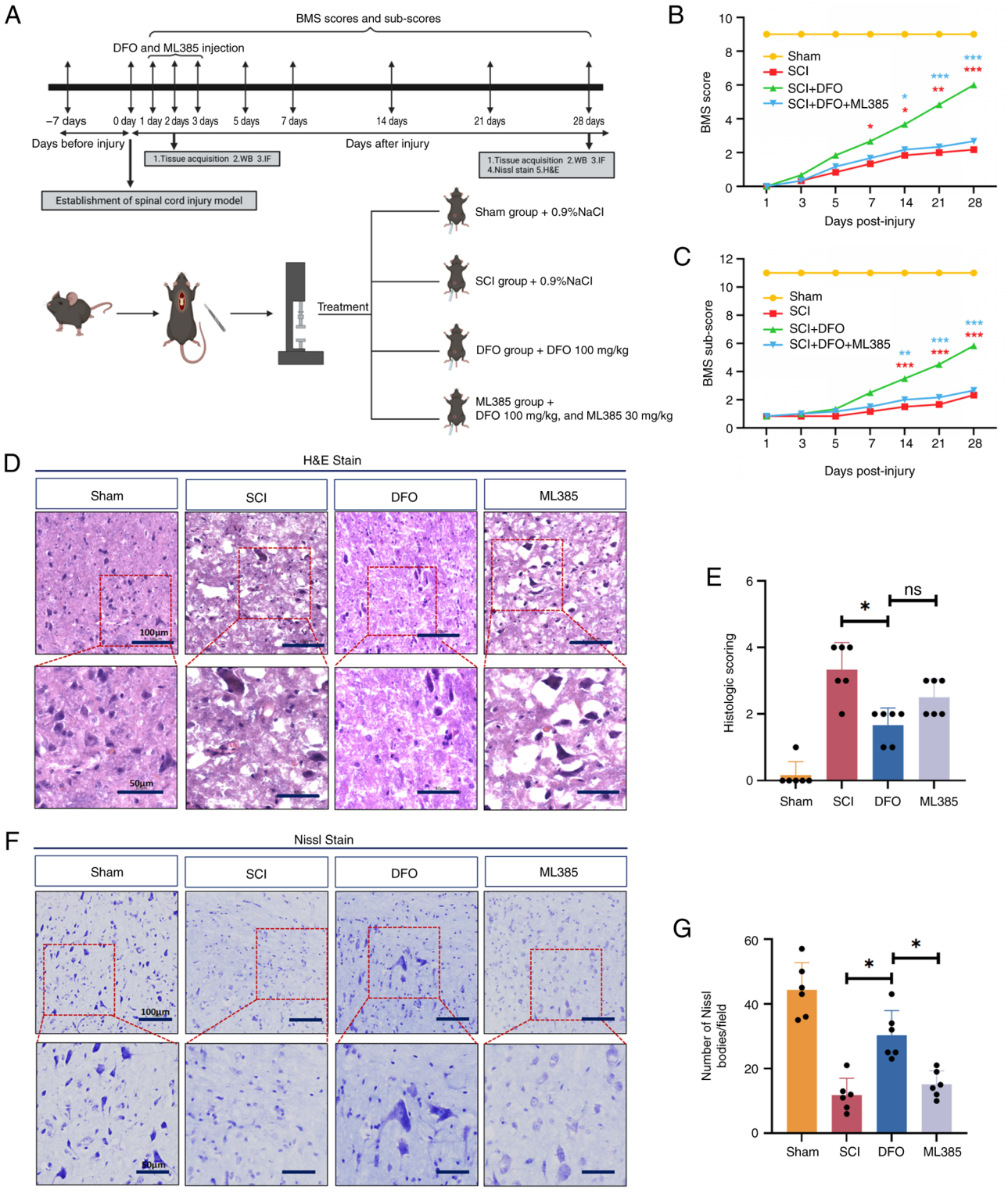

Figure 3. Nrf2 inhibitor ML385 reverses the effects of DFO on the functional and histological recovery of SCI mice. (A) Schematic diagram of the *in vivo* experimental design. (B) BMS score and (C) sub-score were applied to evaluate the recovery of motor function in each group at 1-, 3-, 5-, 7-, 14-, 21- and 28-days post-injury. Data are presented as the mean ± SD (n=6 per group). (D) Representative H&E-stained longitudinal sections of spinal cords from different groups (scale bars, 100 and 50 μm). (E) Quantification of the histopathological changes scored based on edema, neutrophil infiltration and hemorrhage. Data are presented as the mean ± SD (n=6 per group) and were analyzed using one-way ANOVA followed by Bonferroni post hoc test. (F) Nissl staining to observe the number of motor neurons in the anterior horn of the spinal cord (scale bars, 100 and 50 μm). (G) Quantitative analysis of the Nissl body counts. Data are presented as the mean ± SD (n=6 per group) and were analyzed using one-way ANOVA followed by Bonferroni post hoc test. *P<0.05, **P<0.01, ***P<0.001. ns, not significant; DFO, deferoxamine; SCI, spinal cord injury; BMS, Basso Mouse Scale; H&E, hematoxylin and eosin; WB, western blotting; IF, immunofluorescence.

iron metabolism and lipid peroxidation processes at 3 days (subacute phase) and 7 days (early chronic phase) post-SCI, which are hallmark features of ferroptosis.

Volcano plot analysis illustrated the differential gene expression profiles between injured and uninjured spinal cord tissues at 1, 3 and 7 days after SCI (Fig. 6D-F). At 1 day post-injury,

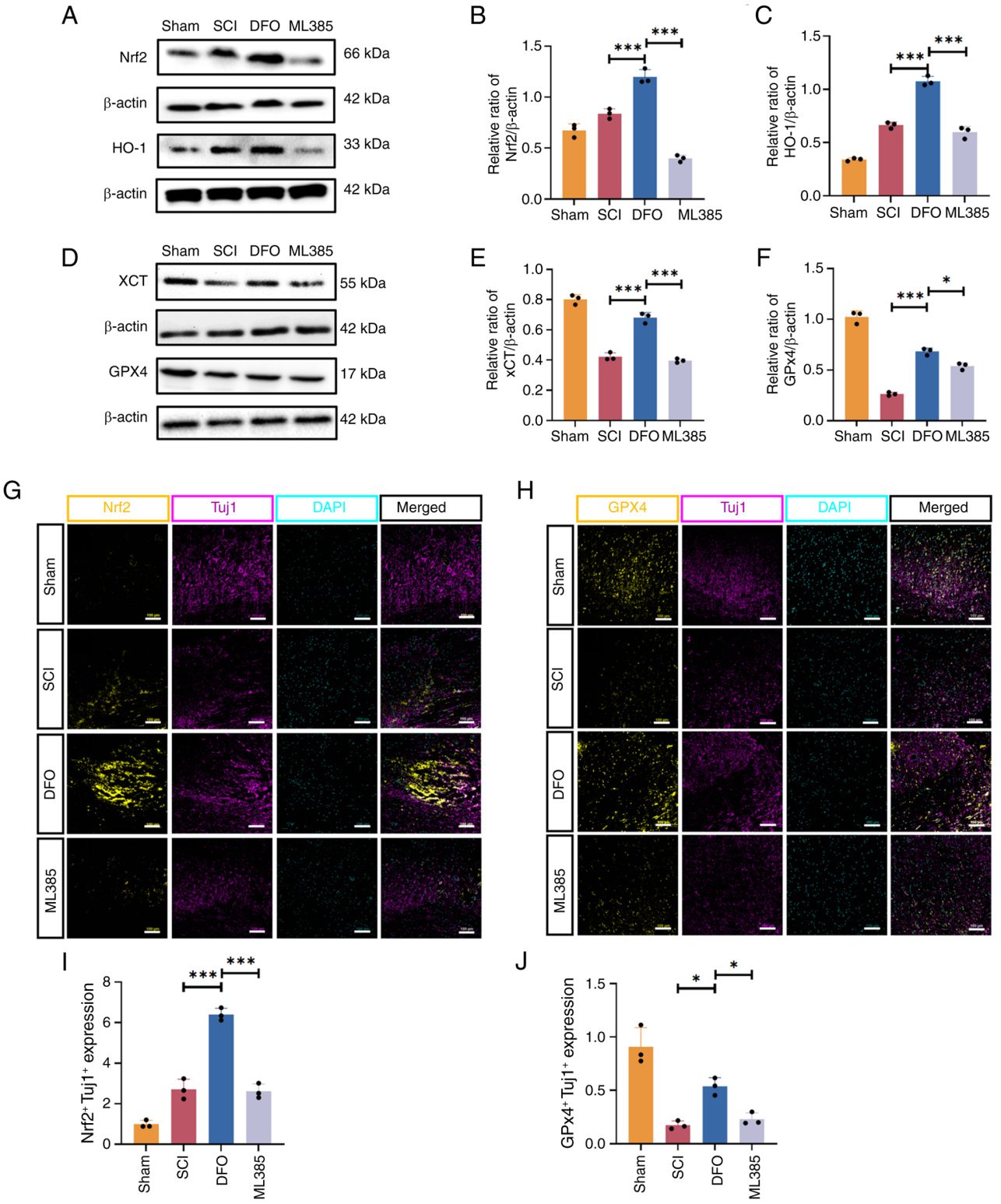

Figure 4. Effects of the Nrf2 inhibitor ML385 on the inhibition of ferroptosis by DFO in SCI mice. (A) Protein expression levels of Nrf2 and HO-1detected by western blotting in different treatment groups with DFO and/or ML385. Semi-quantification of the (B) Nrf2 and (C) HO-1expression levels. (D) Protein expression levels of GPX4 and xCT detected by western blotting in different treatment groups with DFO and/or ML385. (E and F) Semi-quantification of the (E) xCT and (E) GPX4 expression levels. Immunofluorescence staining showing (G) Nrf2 and (H) GPX4 expression in spinal cord samples (scale bar, 100 μm). Quantification of the (I) $Nrf2^{+}Tuj1^{+}$ and (J) $GPX4^{+}Tuj1^{+}$ cells in spinal cord tissue. Data are presented as the mean ± SD (n=3 per group). Statistical analysis was performed using one-way ANOVA followed by Bonferroni post hoc test; $^{*}P<0.05$, $^{***}P<0.001$. DFO, deferoxamine; GPX4, glutathione peroxidase 4; HO-1, heme oxygenase-1; SCI, spinal cord injury; DAPI, 4',6-diamidino-2-phenylindole.

widespread transcriptional changes were observed, reflecting an acute injury response, whereas ferroptosis-related genes showed relatively limited changes. At 3 and 7 days post-SCI, several ferroptosis-related genes showed robust and consistent upregulation. Intersection of the DEGs with curated ferroptosis gene sets identified four representative markers: xCT

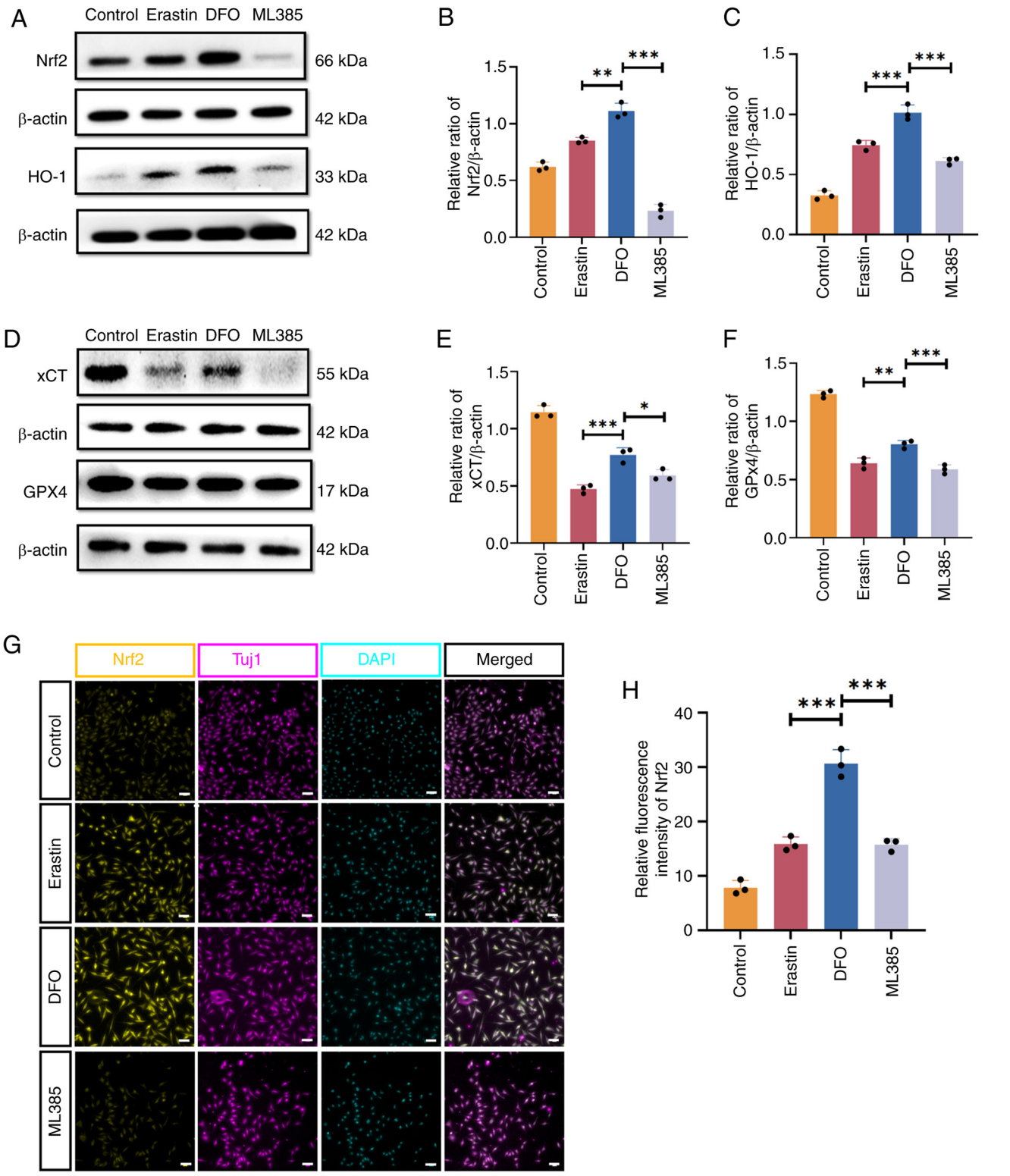

Figure 5. Effects of Nrf2 inhibitor ML385 on the inhibition of ferroptosis by DFO in VSC4.1 cells. (A) Protein expression levels of Nrf2 and HO-1 detected by western blotting in VSC4.1 cells treated with DFO and/or ML385. Semi-quantification of the (B) Nrf2 and (C) HO-1 expression levels. (D) Protein expression levels of GPX4 and xCT detected by western blotting in VSC4.1 cells treated with DFO and/or ML385. (Semi-quantification of the (E) xCT and (F) GPX4 expression levels. (G) Nrf2 expression levels in VSC4.1 cells measured by immunofluorescence staining (scale bar, 50 μm). (H) Quantification of $Nrf2^{+}Tuj1^{+}$ cells in different groups. Data are presented as the mean ± SD (n=3 per group). Statistical analysis was performed using one-way ANOVA followed by Bonferroni post hoc test; $^{*}P<0.05$, $^{**}P<0.01$, $^{***}P<0.001$. DFO, deferoxamine; VSC4.1, ventral spinal cord 4.1; GPX4, glutathione peroxidase 4; HO-1, heme oxygenase-1; DAPI, 4',6-diamidino-2-phenylindole.

(Slc7a11), GPX4, Hmox1 and Nfe2l2 (Nrf2), all of which were significantly upregulated at these later time points, reflecting coordinated activation of antioxidant defense and iron metabolism at 3 and 7 days post-SCI (Fig. 6D-F). Therefore, these genes were selected for further analysis. Temporal expression analysis demonstrated dynamic regulation of these

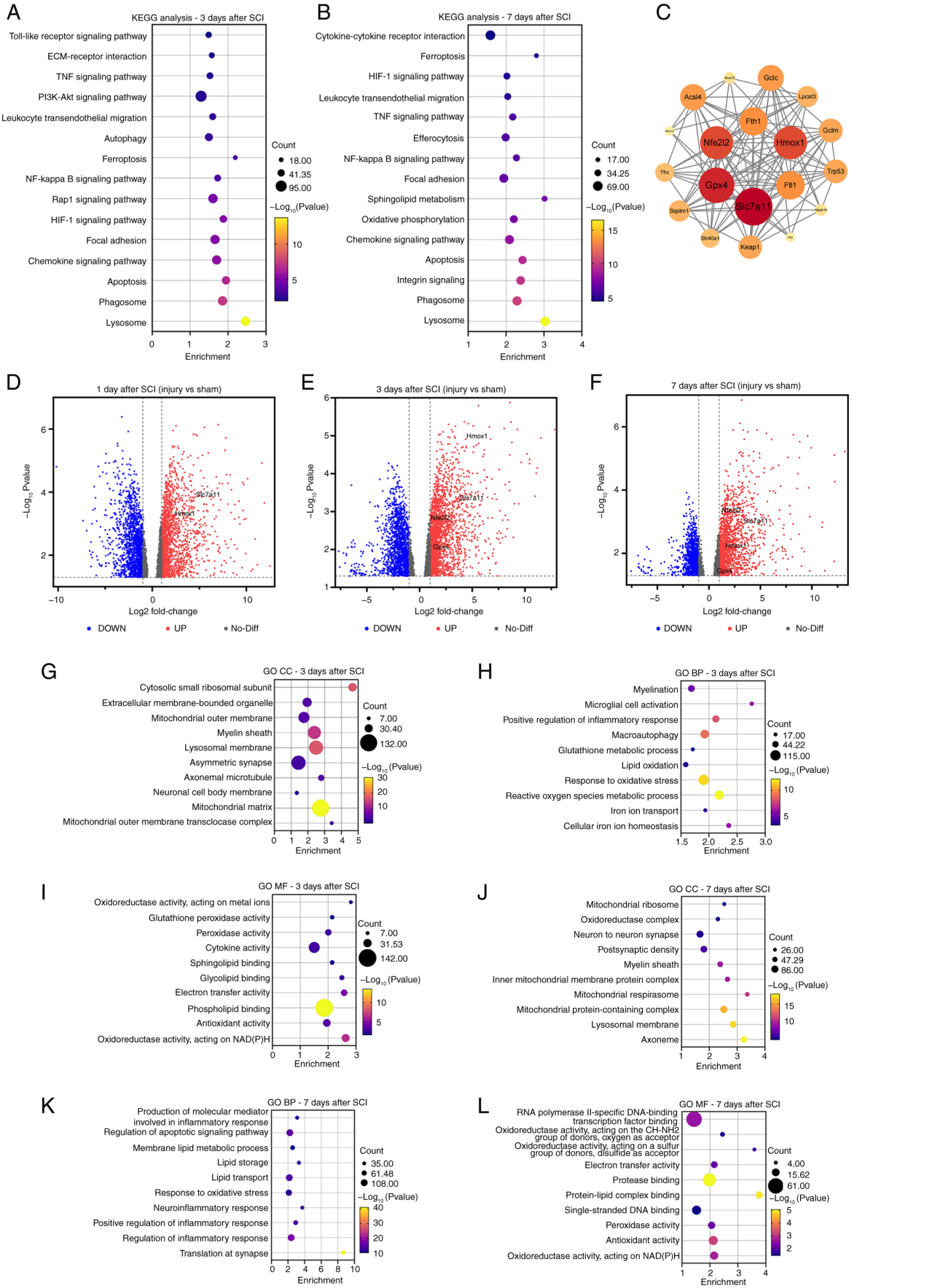

Figure 6. Bioinformatics analysis of DEGs in mouse SCI models. KEGG pathway enrichment analysis for (A) 3 and (B) 7 days post-SCI. (C) Protein-protein interaction network of key ferroptosis-related proteins. Volcano plots showing the DEGs at (D) 1-, (E) 3- and (F) 7-days post-SCI. (G-L) GO enrichment analysis of CC, BP and MF at 3- and 7-days post-SCI. Statistical analysis was performed using a pairwise quasi-likelihood F-test, with a significance threshold of P<0.05, and the pseudo-bulk method was used for differential analysis. DEGs, differentially expressed genes; SCI, spinal cord injury; GO, Gene Ontology; KEGG, Kyoto Encyclopedia of Genes and Genomes; CC, cellular components; BP, biological processes; MF, molecular functions.

genes after SCI (Fig. S1E). Slc7a11, encoding the cystine/glutamate antiporter xCT, was markedly upregulated at 1 day post-SCI, suggesting an early compensatory response aimed at maintaining GSH synthesis. GPX4, a key lipid peroxide scavenger, showed sustained induction at 3 days post-SCI. By contrast, Hmox1 exhibited notable upregulation at later time points, reflecting persistent oxidative stress and iron metabolism dysregulation. Nfe2l2 showed time-dependent activation, consistent with its role as a master regulator of antioxidant and anti-ferroptotic responses. To further explore the regulatory relationships among ferroptosis-associated genes, a PPI interaction network was constructed (Fig. 6C). Network analysis revealed a highly interconnected structure centered on Nfe2l2, Slc7a11 and GPX4, with extensive interactions involving proteins related to iron storage and transport (such as Fth1, Ftl1 and Tfrc), lipid peroxidation (such as Acsl4, Alox12 and Alox15) and GSH metabolism (such as Gclc, Gclm and Gss). After SCI, ferroptosis-related proteins showed close functional associations, centering on the Nrf2/xCT/GPX4 pathway rather than acting in isolation.

Discussion

The present study explored the role of the Nrf2/HO-1 signaling pathway in mediating the inhibitory effects of DFO on neuronal ferroptosis following SCI. The findings revealed an upregulation of Nrf2 and HO-1 expression after SCI and DFO treatment in mice, corroborated by *in vitro* experiments demonstrating increased Nrf2 and HO-1 levels following DFO administration in an erastin-induced neuronal ferroptosis model. Employing the Nrf2 inhibitor ML385, it was demonstrated that blocking Nrf2 reversed the inhibitory effects of DFO on ferroptosis in both SCI mice and VSC4.1 cells. Notably, ML385 also attenuated the functional recovery of SCI mice under DFO treatment. Collectively, these findings underscore the role of DFO in promoting functional recovery after SCI by mitigating neuronal ferroptosis through activation of the Nrf2/HO-1 signaling pathway (Fig. 7).

Ferroptosis, a recently identified type of cell death, has emerged as a critical contributor to SCI pathology, as substantiated by our prior research (12) and other investigations in the field (6,14). DFO, an iron chelator, has shown potential in enhancing functional and histological recovery after SCI by mitigating ferroptosis (12). Expanding upon these findings, our previous study further delineated the inhibitory effects of DFO on erastin-induced neuronal ferroptosis *in vitro* (17). The role of ferroptosis in SCI has gained increasing attention. Ni *et al* (20) demonstrated that resveratrol promotes functional recovery and attenuates ferroptosis post-SCI. Zou *et al* (16) reported the promotion of neuronal ferroptosis and M1 macrophage polarization in SCI, highlighting the potential inhibitory role of protein arginine methyltransferase 8 via regulation of glial cell-derived neurotrophic factor expression. Additionally, Li *et al* (31) provided evidence suggesting that dihydroorotate dehydrogenase, a potent inhibitor of ferroptosis in tumor cells, may also play a role in mitigating neuronal ferroptosis following SCI (32). Given the mounting evidence implicating ferroptosis in SCI pathogenesis, targeting this pathway presents a promising avenue for therapeutic intervention.

To advance the clinical translation of drug therapy for SCI, it is imperative to elucidate the molecular mechanisms comprehensively. The present study provides evidence that DFO fosters functional recovery and mitigates neuronal ferroptosis by modulating the Nrf2/HO-1 signaling pathway following SCI. Notably, the Nrf2/HO-1 pathway is well recognized in SCI research. For instance, curcumin, a medicinal plant agent, has been reported to mitigate inflammatory damage by scavenging free radicals and activating Nrf2/HO-1 to facilitate SCI repair (33). Moreover, deficiency in the Pregnane X receptor has been shown to activate the Nrf2/HO-1 pathway, conferring protection against SCI (34). Several studies have explored the role of Nrf2 in regulating ferroptosis (19,35). Gong *et al* (19) concluded that trehalose inhibits ferroptosis through the Nrf2/HO-1 pathway, promoting functional recovery in SCI mice. In addition to its involvement in ferroptosis, Nrf2 also modulates other biological processes in SCI, such as microglial polarization, neuroinflammation and oxidative stress (36,37). Notably, the expression of Nrf2 and HO-1 were upregulated following SCI in the present study. This might be attributed to the body's response to increased oxidative stress and inflammation, which are key components of the secondary injury phase after SCI. Hence, the upregulation of Nrf2 and HO-1 after SCI might represent the body's attempt to limit the extent of damage and promote recovery. Although the present study did not directly investigate these processes, it highlights the need for further research into the regulatory effects of DFO on various biological processes through the activation of Nrf2/HO-1. Such investigations could provide deeper insights into the multifaceted therapeutic mechanisms underlying DFO treatment in SCI. Besides, although Nrf2/HO-1 is a well-known pathway involved in oxidative stress responses, its precise role in the context of the inhibitory effects of DFO on ferroptosis after SCI has not been fully elucidated. The present study advances the current understanding by providing novel insights into how DFO modulates this critical pathway to mitigate neuronal damage in SCI. To the best of our knowledge, the present study is the first to demonstrate that the efficacy of DFO in reducing ferroptosis may be closely linked to the activation of Nrf2/HO-1, which may subsequently lead to enhanced antioxidant defense mechanisms and improved functional recovery. This novel mechanistic insight not only deepens our understanding of the therapeutic action of DFO but also opens new avenues for targeted interventions in SCI treatment, making the findings both innovative and notable in the field of neuroprotection.

The spinal cord tissue comprises several types of cells, including neurons, astrocytes, oligodendrocytes and microglia. Notably, all these cell types are susceptible to ferroptosis, a form of regulated cell death characterized by lipid peroxidation. For instance, in Alzheimer's disease, NADPH oxidase 4 induces ferroptosis in astrocytes through oxidative stress-induced lipid peroxidation, leading to mitochondrial dysfunction (38). Similarly, ferroptosis in oligodendrocyte progenitor cells contributes to white matter injury following hemorrhagic stroke, suggesting that targeting ferroptotic oligodendrocytes could be a therapeutic approach for stroke and related conditions (39). Spinal cord neurons play crucial roles as cellular connections between the brain and the body, influencing behavior regulation and pathological conditions.

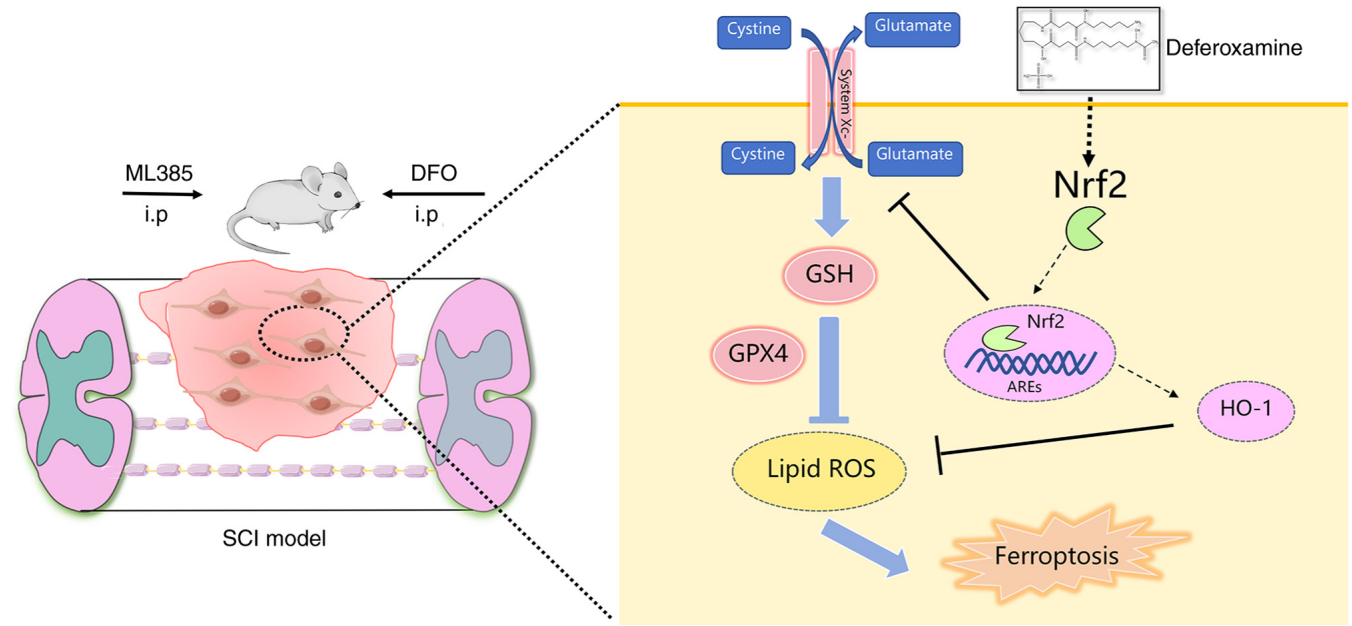

Figure 7. Proposed regulatory mechanism of DFO in SCI mice. DFO, deferoxamine; SCI, spinal cord injury; i.p., intraperitoneal; GSH, glutathione; glutathione peroxidase 4; HO-1, heme oxygenase-1; ROS, reactive oxygen species; AREs, antioxidant response elements.

Given their importance, neuronal survival or loss directly impacts functional recovery in SCI. Therefore, the present study primarily focused on investigating ferroptosis in neurons. To assess ferroptosis in spinal cord neurons, Tuj1 was utilized as a marker for neuronal labeling. The findings revealed an increase in $GPX4^{+}Tuj1^{+}$ neurons in spinal cord tissue following DFO administration, indicative of a protective effect against ferroptosis. Several studies have shown that neuronal ferroptosis plays a vital role in SCI pathology (40,41). Conversely, interference with Nrf2 using ML385 led to a decrease in $GPX4^{+}Tuj1^{+}$ neurons, suggesting a disruption of the protective mechanism. In the present study, the VSC4.1 cell line, a hybrid motor neuron cell line created through the fusion of a mice ventral spinal cord neuron with a mouse neuroblastoma cell line (42), was employed to establish a neuronal ferroptosis model using erastin. The results demonstrated that under the experimental conditions used in the present study (Control and erastin ± DFO ± ML385), VSC4.1 cells were Tuj1-positive and showed detectable Nrf2 and GPX4 expression, supporting their use as an *in vitro* neuronal model for ferroptosis-related analyses. However, it is essential to acknowledge that the focus of the present study on neuronal ferroptosis has limited the comprehensive understanding of ferroptosis processes in other cell types following SCI. In addition to neurons, accumulating data indicate that ferroptosis in glial cells also contributes to the complex pathology of SCI (43-45). Oligodendrocytes, which are enriched in polyunsaturated phospholipids and display relatively high intracellular iron levels, are particularly susceptible to ferroptotic injury after central nervous system trauma (46). Experimental SCI models have demonstrated that iron accumulation and lipid peroxidation within oligodendrocytes are closely associated with secondary white-matter damage, and pharmacological inhibition of ferroptosis (such as by ferrostatin-1 or liproxstatin-1) reduces oligodendrocyte loss, alleviates white-matter injury and improves locomotor recovery (47,48). Moreover, astrocytes and microglia exhibit ferroptosis-related changes after SCI, and astrocyte-specific activation of Nrf2 has been shown to attenuate oxidative stress, demyelination and neurological dysfunction, underscoring the importance of glial antioxidant and ferroptosis-regulating pathways in shaping the injury milieu (49). Given that DFO is a potent iron chelator and ferroptosis inhibitor, its beneficial effects in the SCI model established in the present study are likely not restricted to neurons. Previous work has demonstrated that systemic DFO treatment after SCI decreases iron overload, restores GPX4/xCT/GSH expression, improves behavioral recovery and concurrently enhances neuronal survival while inhibiting gliosis, suggesting coordinated protection of both neuronal and glial compartments (12). Together with the present findings, these observations support the notion that DFO may modulate ferroptosis across multiple spinal cord cell types, which including neurons, oligodendrocytes and astrocytes, through iron chelation and Nrf2-dependent antioxidant mechanisms. Future studies should consider investigating ferroptosis across various cell types to provide a more comprehensive acknowledgement of its role in SCI pathogenesis.

The demonstration by the present study that DFO can effectively mitigate neuronal ferroptosis and promote functional recovery by activating the Nrf2/HO-1 pathway suggests that DFO or similar agents could be integrated into current SCI treatment paradigms. Given that DFO is an FDA-approved iron chelator indicated for acute iron intoxication and transfusional iron overload in patients with chronic anemia, its repurposing for SCI treatment could offer a more expedited pathway toward clinical translation. Beyond ferroptosis inhibition, DFO has also been reported to attenuate key components of secondary injury after SCI, including oxidative/nitrosative stress (such as reduced lipid peroxidation/MDA and nitrotyrosine formation) and inflammation (such as reduced neutrophil infiltration,

NF-κB activation and iNOS expression), thereby contributing to tissue protection and improved functional outcomes in preclinical models (50). However, the clinical translation of these findings will require careful consideration of several challenges. First, the optimal dosing and timing of DFO administration must be established to maximize therapeutic efficacy while minimizing potential side effects, such as infusion-related hypotension/hypersensitivity and dose-dependent auditory/ocular toxicities, which warrant careful safety monitoring in translational studies (51). Additionally, the long-term effects of DFO treatment on neuroregeneration and functional outcomes in patients with SCI need to be thoroughly evaluated through clinical trials. Another challenge lies in understanding the interaction of DFO with other cell types within the spinal cord, such as astrocytes and microglia, which also play crucial roles in SCI pathology. Addressing these challenges through rigorous preclinical and clinical studies will be essential for translating the findings of the present study into effective clinical interventions.

Previous transcriptomic analyses of public datasets have shown that multiple regulated cell death pathways, including pyroptosis, necroptosis and hypoxia-related injury, are actively involved in shaping the post-injury microenvironment and inflammatory response after SCI (52-55). To further characterize ferroptosis over time, the present study applied a time-resolved, ferroptosis-centered transcriptomic analysis based on a publicly available GEO dataset (GSE162610), including differential expression analysis, KEGG enrichment, GO annotation and PPI network construction. At 1 day (acute phase), 3 days (subacute phase) and 7 days (early chronic phase) post-SCI, ferroptosis-associated signaling was consistently linked to oxidative stress, lipid peroxidation, iron metabolism dysregulation and mitochondrial dysfunction, which are hallmark features of secondary injury following SCI. KEGG analysis showed a progressive enrichment of ferroptosis-related pathways after injury, while GO analysis further linked these changes to GSH metabolism, antioxidant defense, iron homeostasis and mitochondrial and lysosomal functions. Notably, the PPI network further revealed that these diverse processes are integrated through a tightly connected regulatory core centered on the Nrf2/xCT/GPX4 axis. Within this network, Nfe2l2 (Nrf2) occupies a central transcriptional position linking upstream redox sensing (Keap1) with downstream antioxidant and ferroptosis-suppressing targets (Slc7a11, Gpx4 and Hmox1). This systems-level organization suggests that activation of Nrf2-dependent signaling represents an endogenous compensatory mechanism aimed at counteracting ferroptosis after SCI. However, in the time-resolved analyses, despite upregulation of antioxidant/anti-ferroptotic genes (such as Nfe2l2/Nrf2, Slc7a11/xCT, Gpx4 and Hmox1), the KEGG term 'Ferroptosis' remained significantly enriched at 3 and 7 days post-SCI and GO enrichment continued to highlight 'lipid oxidation' and 'cellular iron ion homeostasis'. Together with the PPI network implicating iron-handling and lipid-peroxidation nodes (such as Fth1/Ftl1/Tfrc, Acsl4 and Alox12/15), these findings suggest that endogenous defenses are insufficient to fully restrain persistent ferroptosis-associated injury. Given that DFO is a potent iron chelator and ferroptosis inhibitor, we hypothesized that its neuroprotective effects after SCI might be mediated through activation of the Nrf2/HO-1/xCT/GPX4 axis. Accordingly, complementary *in vivo* and *in vitro* experiments were performed to test the causal involvement of ferroptosis and Nrf2 signaling in neuronal protection after SCI. When integrated with the transcriptomic evidence of regulated cell-death programs, the present study supports a mechanistic model in which DFO confers neuroprotection primarily by suppressing ferroptotic injury through Nrf2-dependent antioxidant regulation, with downstream responses becoming particularly prominent during the subacute phase (3 days post-SCI). Although the xCT/GPX4 axis was validated experimentally, the relative contributions and interactions of additional Nrf2-regulated targets remain to be clarified. Future work using cell-type-resolved profiling (such as single-cell or spatial transcriptomics) together with targeted perturbation of prioritized downstream nodes will help define the regulatory hierarchy of Nrf2-controlled ferroptosis and refine therapeutic strategies.

Several limitations of the present study should be acknowledged. First, the *in vitro* experiments performed in the present study relied on the VSC4.1 neuronal cell line, which may not fully recapitulate the morphological and functional complexity of primary neurons, potentially limiting translational relevance. Second, the *in vivo* experiments were conducted exclusively in female mice, which may introduce sex-specific bias and limit generalizability across sexes. In addition, despite efforts to standardize the injury procedure, inherent variability in animal models of SCI may contribute to outcome heterogeneity. Furthermore, in the present study, the experimental interventions primarily assessed the necessity of Nrf2 signaling through pharmacological inhibition and complementary activation strategies using Nrf2 agonists were not explored. Finally, the present study focused mainly on neuronal responses, without fully addressing interactions with other spinal cord cell types, such as astrocytes and microglia, which are known to influence ferroptosis and secondary injury after SCI. Future studies incorporating cell-specific omics approaches, pathway activation strategies and multicellular interaction analyses will be important to further refine the translational potential of targeting Nrf2-regulated ferroptosis in SCI.

In summary, the present study demonstrated that DFO mitigated neuronal ferroptosis and improved functional recovery after SCI in part by activating the Nrf2/HO-1 signaling pathway and enhancing the xCT/GPX4 antioxidant system. These results support DFO as a potential therapeutic agent for SCI and highlight Nrf2-dependent anti-ferroptotic mechanisms as promising targets for future therapeutic strategies.

Acknowledgements

Not applicable.

Funding

This work was supported by the Beijing Tongzhou District Science and Technology Project (grant no. KJ2023SS013), the Youth Scientific Research Incubation Program of Beijing Luhe Hospital, Capital Medical University (grant no. LHYY-JC104) and the Beijing-Tianjin-Hebei Basic Research Cooperation Project (grant no. J230012).

Availability of data and materials

The data generated in the present study may be requested from the corresponding author.

Authors' contributions

YZ, LL and XMC conceived and designed the study, supervised the project and acquired funding. ZQM, XWZ, XY and TL established the SCI model, conducted the animal experiments and drug interventions and performed the primary data acquisition. BQT carried out the behavioral assessments (including BMS scoring) and contributed to the acquisition of functional outcome data. ZQM and XWZ performed the molecular assays (including protein and/or gene expression analyses), acquired the associated data and participated in data processing. TL, GHL and HYZ conducted the histological and immunofluorescence analyses and performed the quantitative image-based measurements. YZ, LL and XMC performed the statistical analyses and assisted with data interpretation. XWZ and ZQM contributed to experimental procedures, data collection and prepared the figures. YZ, XY and BQT analyzed and interpreted the data and drafted the initial manuscript. XMC, ZQM and XWZ critically revised the manuscript for important intellectual content. YZ and XMC confirm the authenticity of all the raw data. All authors read and approved the final version of the manuscript.

Ethics approval and consent to participate

Animal experiments were conducted in accordance with the laboratory animal management guidelines. All animal experimental procedures were approved by the Animal Experiments and Experimental Animal Welfare Committee of Capital Medical University (approval no. AEEI-2023-029).

Patient consent for publication

Not applicable.

Competing interests

The authors declare that they have no competing interests.

Authors' information

ORCID: Xueming Chen, 0009-0001-8681-9660; Xinwei Zhang, 0009-0003-3182-4758; Ziqian Ma, 0000-0003-1245-378X

References

1. Golestani A, Shobeiri P, Sadeghi-Naini M, Jazayeri SB, Maroufi SF, Ghodsi Z, Dabbagh Ohadi MA, Mohammadi E, Rahimi-Movaghar V and Ghodsi SM: Epidemiology of traumatic spinal cord injury in developing countries from 2009 to 2020: A systematic review and meta-analysis. Neuroepidemiology 56: 219-239, 2022.
2. Tubbs RS, Blouir MC, Romeo AK, Mortazavi MM and Cohen-Gadol AA: Spinal cord ischemia and atherosclerosis: A review of the literature. Br J Neurosurg 25: 666-670, 2011.
3. Quadri SA, Farooqui M, Ikram A, Zafar A, Khan MA, Suriya SS, Claus CF, Fiani B, Rahman M, Ramachandran A, *et al*: Recent update on basic mechanisms of spinal cord injury. Neurosurg Rev 43: 425-441, 2020.
4. Choo AM, Liu J, Lam CK, Dvorak M, Tetzlaff W and Oxland TR: Contusion, dislocation, and distraction: Primary hemorrhage and membrane permeability in distinct mechanisms of spinal cord injury. J Neurosurg Spine 6: 255-266, 2007.
5. Ahuja CS, Wilson JR, Nori S, Kotter MRN, Druschel C, Curt A and Fehlings MG: Traumatic spinal cord injury. Nat Rev Dis Primers 3: 17018, 2017.
6. Li S, Gao S, Hu Y, Sun G, Feng J and Sheng W: Ferroptosis in spinal cord injury: Research progress and novel insights. J Cell Biochem 126: e70067, 2025.
7. Yu T, Yang LL, Zhou Y, Wu MF and Jiao JH: Exosome-mediated repair of spinal cord injury: A promising therapeutic strategy. Stem Cell Res Ther 15: 6, 2024.
8. Zhiguo F, Ji W, Shenyuan C, Guoyou Z, Chen K, Hui Q, Wenrong X and Zhai X: A swift expanding trend of extracellular vesicles in spinal cord injury research: A bibliometric analysis. J Nanobiotechnology 21: 289, 2023.
9. Shi Z, Yuan S, Shi L, Li J, Ning G, Kong X and Feng S: Programmed cell death in spinal cord injury pathogenesis and therapy. Cell Prolif 54: e12992, 2021.
10. Dixon SJ, Lemberg KM, Lamprecht MR, Skouta R, Zaitsev EM, Gleason CE, Patel DN, Bauer AJ, Cantley AM, Yang WS, *et al*: Ferroptosis: An iron-dependent form of nonapoptotic cell death. Cell 149: 1060-1072, 2012.
11. Li FJ, Long HZ, Zhou ZW, Luo HY, Xu SG and Gao LC: System X_c^-/GSH/GPX4 axis: An important antioxidant system for the ferroptosis in drug-resistant solid tumor therapy. Front Pharmacol 13: 910292, 2022.
12. Yao X, Zhang Y, Hao J, Duan HQ, Zhao CX, Sun C, Li B, Fan BY, Wang X, Li WX, *et al*: Deferoxamine promotes recovery of traumatic spinal cord injury by inhibiting ferroptosis. Neural Regen Res 14: 532-541, 2019.
13. Zhang Y, Sun C, Zhao C, Hao J, Zhang Y, Fan B, Li B, Duan H, Liu C, Kong X, *et al*: Ferroptosis inhibitor SRS 16-86 attenuates ferroptosis and promotes functional recovery in contusion spinal cord injury. Brain Res 1706: 48-57, 2019.
14. Bai XY, Liu XL, Deng ZZ, Wei DM, Zhang D, Xi HL, Wang QY, He MZ and Yang YL: Ferroptosis is a new therapeutic target for spinal cord injury. Front Neurosci 17: 1136143, 2023.
15. Wang C, Zhu Y, Zhu X, Chen R, Zhang X and Lian N: USP7 regulates HMOX-1 via deubiquitination to suppress ferroptosis and ameliorate spinal cord injury in rats. Neurochem Int 168: 105554, 2023.
16. Zou Z, Liu R, Wang Y, Tan H, An G, Zhang B, Wang Y and Dong D: Protein arginine methyltransferase 8 regulates ferroptosis and macrophage polarization in spinal cord injury via glial cell-derived neurotrophic factor. CNS Neurosci Ther 29: 2145-2161, 2023.
17. Zhang Y, Fan BY, Pang YL, Shen WY, Wang X, Zhao CX, Li WX, Liu C, Kong XH, Ning GZ, *et al*: Neuroprotective effect of deferoxamine on erastininduced ferroptosis in primary cortical neurons. Neural Regen Res 15: 1539-1545, 2020.
18. Ge MH, Tian H, Mao L, Li DY, Lin JQ, Hu HS, Huang SC, Zhang CJ and Mei XF: Zinc attenuates ferroptosis and promotes functional recovery in contusion spinal cord injury by activating Nrf2/GPX4 defense pathway. CNS Neurosci Ther 27: 1023-1040, 2021.
19. Gong F, Ge T, Liu J, Xiao J, Wu X, Wang H, Zhu Y, Xia D and Hu B: Trehalose inhibits ferroptosis via NRF2/HO-1 pathway and promotes functional recovery in mice with spinal cord injury. Aging (Albany NY) 14: 3216-3232, 2022.
20. Ni C, Ye Q, Mi X, Jiao D, Zhang S, Cheng R, Fang Z, Fang M and Ye X: Resveratrol inhibits ferroptosis via activating NRF2/GPX4 pathway in mice with spinal cord injury. Microsc Res Tech 86: 1378-1390, 2023.
21. Li Z, Cheng P, Xi H, Jiang T, Zheng X, Qiu J, Gong Y, Wu X, Mi S, Hong Y, *et al*: Tomatidine alleviates intervertebral disc degeneration by activating the Nrf2/HO-1/GPX4 signaling pathway. Drug Des Devel Ther 18: 6313-6329, 2024.
22. Liu D, Yang S and Yu S: Interactions between ferroptosis and oxidative stress in ischemic stroke. Antioxidants (Basel) 13: 1329, 2024.
23. Percie du Sert N, Hurst V, Ahluwalia A, Alam S, Avey MT, Baker M, Browne WJ, Clark A, Cuthill IC, Dirnagl U, *et al*: The ARRIVE guidelines 2.0: Updated guidelines for reporting animal research. BMJ Open Sci 4: e100115, 2020.
24. Zhang X, Liu T, Ma Z, Li G, Ding N, Wang Z, Guan Y, Zhang Y, Liu L and Chen X: VEGF secreted by human dental pulp stem cell promotes spinal cord injury repair by inhibiting microglial pyroptosis through the PI3K/AKT pathway. J Transl Med 23: 437, 2025.

25. Xian P, Hei Y, Wang R, Wang T, Yang J, Li J, Di Z, Liu Z, Baskys A, Liu W, *et al*: Mesenchymal stem cell-derived exosomes as a nanotherapeutic agent for amelioration of inflammation-induced astrocyte alterations in mice. Theranostics 9: 5956-5975, 2019.
26. Basso DM, Fisher LC, Anderson AJ, Jakeman LB, McTigue DM and Popovich PG: Basso mouse scale for locomotion detects differences in recovery after spinal cord injury in five common mouse strains. J Neurotrauma 23: 635-659, 2006.
27. Liu T, Ma Z, Liu L, Pei Y, Wu Q, Xu S, Liu Y, Ding N, Guan Y, Zhang Y and Chen X: Conditioned medium from human dental pulp stem cells treats spinal cord injury by inhibiting microglial pyroptosis. Neural Regen Res 19: 1105-1111, 2024.
28. Kim HJ, Im W, Kim S, Kim SH, Sung JJ, Kim M and Lee KW: Calcium-influx increases SOD1 aggregates via nitric oxide in cultured motor neurons. Exp Mol Med 39: 574-582, 2007.
29. Choi JH, Jang M, Lee JI, Chung WS and Cho IH: Neuroprotective effects of a traditional multi-herbal medicine kyung-ok-ko in an animal model of Parkinson's disease: Inhibition of MAPKs and NF-κB pathways and activation of keap1-Nrf2 pathway. Front Pharmacol 9: 1444, 2018.
30. Milich LM, Choi JS, Ryan C, Cerqueira SR, Benavides S, Yahn SL, Tsoulfas P and Lee JK: Single-cell analysis of the cellular heterogeneity and interactions in the injured mouse spinal cord. J Exp Med 218: e20210040, 2021.
31. Li D, Lu X, Xu G, Liu S, Gong Z, Lu F, Xia X, Jiang J, Wang H, Zou F and Ma X: Dihydroorotate dehydrogenase regulates ferroptosis in neurons after spinal cord injury via the P53-ALOX15 signaling pathway. CNS Neurosci Ther 29: 1923-1939, 2023.
32. Zavvarian MM, Hong J and Fehlings MG: The functional role of spinal interneurons following traumatic spinal cord injury. Front Cell Neurosci 14: 127, 2020.
33. Jin W, Botchway BOA and Liu X: Curcumin can activate the Nrf2/HO-1 signaling pathway and scavenge free radicals in spinal cord injury treatment. Neurorehabil Neural Repair 35: 576-584, 2021.
34. Xuan LN, Hu ZX, Jiang ZF, Zhang C, Sun XW, Ming WH, Liu HT, Qiao RF, Shen LJ, Liu SB, *et al*: Pregnane X receptor (PXR) deficiency protects against spinal cord injury by activating NRF2/HO-1 pathway. CNS Neurosci Ther 29: 3460-3478, 2023.
35. Song X and Long D: Nrf2 and ferroptosis: A new research direction for neurodegenerative diseases. Front Neurosci 14: 267, 2020.
36. Luo Y, He YZ, Wang YF, Xu YX and Yang L: Adipose-derived mesenchymal stem cell exosomes ameliorate spinal cord injury in rats by activating the Nrf2/HO-1 pathway and regulating microglial polarization. Folia Neuropathol 61: 326-335, 2023.
37. Zhang X, Xu L, Chen X, Zhou X and Cao L: Acacetin alleviates neuroinflammation and oxidative stress injury via the Nrf2/HO-1 pathway in a mouse model of spinal cord injury. Transl Neurosci 13: 483-494, 2022.
38. Park MW, Cha HW, Kim J, Kim JH, Yang H, Yoon S, Boonpraman N, Yi SS, Yoo ID and Moon JS: NOX4 promotes ferroptosis of astrocytes by oxidative stress-induced lipid peroxidation via the impairment of mitochondrial metabolism in Alzheimer's diseases. Redox Biol 41: 101947, 2021.
39. Shen D, Wu W, Liu J, Lan T, Xiao Z, Gai K, Hu L, Luo Z, Wei C, Wang X, *et al*: Ferroptosis in oligodendrocyte progenitor cells mediates white matter injury after hemorrhagic stroke. Cell Death Dis 13: 259, 2022.
40. Xu T, Zhu Q, Huang Q, Gu Q, Zhu Y, Tang M, Tian S, Wang L, Yan F, Ge J, *et al*: FGF21 prevents neuronal cell ferroptosis after spinal cord injury by activating the FGFR1/β-Klotho pathway. Brain Res Bull 202: 110753, 2023.
41. Xiao S, Zhang Y, Wang S, Liu J, Dan F, Yang F, Hong S, Liu N, Zeng Y, Huang K, *et al*: The Syvn1 inhibits neuronal cell ferroptosis by activating Stat3/Gpx4 axis in rat with spinal cord injury. Cell Prolif 57: e13658, 2024.
42. Alexianu ME, Mohamed AH, Smith RG, Colom LV and Appel SH: Apoptotic cell death of a hybrid motoneuron cell line induced by immunoglobulins from patients with amyotrophic lateral sclerosis. J Neurochem 63: 2365-2368, 1994.
43. Song Q, Cui Q, Sun S, Wang Y, Yuan Y and Zhang L: Crosstalk between cell death and spinal cord injury: Neurology and therapy. Mol Neurobiol 61: 10271-10287, 2024.
44. Li L, Cao Y, Zhang X, Guo J, Lin Z, Zhou P, Chen C, Chen J, Liu Y, Luo D, *et al*: Injectable ROS homeostasis protective hydrogel inhibiting microglial ferroptosis through the Nrf2/Slc7a11/Gpx4 to alleviate neuropathic pain and promote spinal cord injury repair. Redox Biol 86: 103816, 2025.
45. Liang X, Qin R, Qin Q, Xu W, Xu H, Lai X, Shao L, Li C, Xie M, Xiong X, *et al*: Therapeutic potential of astrocyte transdifferentiated neurons. Neural Regen Res: Dec 30, 2025 (Epub ahead of print).
46. Li F, Wang H, Chen H, Guo J, Dang X, Ru Y and Wang H: Mechanism of ferroptosis and its role in spinal cord injury. Front Neurol 13: 926780, 2022.
47. Ge H, Xue X, Xian J, Yuan L, Wang L, Zou Y, Zhong J, Jiang Z, Shi J, Chen T, *et al*: Ferrostatin-1 Alleviates white matter injury via decreasing ferroptosis following spinal cord injury. Mol Neurobiol 59: 161-176, 2022.
48. Li Y, Cao Y, Xiao J, Shang J, Tan Q, Ping F, Huang W, Wu F, Zhang H and Zhang X: Inhibitor of apoptosis-stimulating protein of p53 inhibits ferroptosis and alleviates intestinal ischemia/reperfusion-induced acute lung injury. Cell Death Differ 27: 2635-2650, 2020.
49. Zhao W, Gasterich N, Clarner T, Voelz C, Behrens V, Beyer C, Fragoulis A and Zendedel A: Astrocytic Nrf2 expression protects spinal cord from oxidative stress following spinal cord injury in a male mouse model. J Neuroinflammation 19: 134, 2022.
50. Paterniti I, Mazzon E, Emanuela E, Paola RD, Galuppo M, Bramanti P and Cuzzocrea S: Modulation of inflammatory response after spinal cord trauma with deferoxamine, an iron chelator. Free Radic Res 44: 694-709, 2010.
51. Yi Y, Jia P, Xie P, Peng X, Zhu X, Yin S, Luo Y, Deng Y and Wan L: Beyond oxidative stress: Ferroptosis as a novel orchestrator in neurodegenerative disorders. Front Immunol 16: 1683876, 2025.
52. Cheng S, Li L, Xu M, Ma N and Zheng Y: Exploring hypoxia-related genes in spinal cord injury: A pathway to new therapeutic targets. Front Mol Neurosci 18: 1565430, 2025.
53. Liu J, Cao J, Yu X, Chang J, Sui T and Cao X: Necroptosis pathway emerged as potential diagnosis markers in spinal cord injury. J Cell Mol Med 28: e18219, 2024.
54. Lu F, Liu Y, Chen Z, Chen S, Liang W, Hua F, Zhong M and Wang L: Identification and validation of glucocorticoid receptor and programmed cell death-related genes in spinal cord injury using machine learning. Sci Rep 15: 24202, 2025.
55. Xiang-Xia, Li KX, Li QW, Wu ZM, Guo RC and Shen CL: Identifying pyroptosis- and inflammation-related genes in spinal cord injury based on bioinformatics analysis. Sci Rep 15: 25424, 2025.